


Non-Hermitian unidirectional routing of photonic qubitsEn-Ze Li,^{1,2,‡} Yi-Yang Liu^{3,‡} Ming-Xin Dong,^{1,2} Dong-Sheng Ding^{1,2,4,*} and Bao-Sen Shi^{1,2,4,†}¹*Key Laboratory of Quantum Information, University of Science and Technology of China, Hefei, 230026 Anhui, China*²*Synergetic Innovation Center of Quantum Information and Quantum Physics, University of Science and Technology of China, Hefei, 230026 Anhui, China*³*School of Physical Science and Technology, Lanzhou University, Lanzhou, 730000 Gansu, China*⁴*Hefei National Laboratory, Hefei, 230088 Anhui, China* (Received 24 September 2023; revised 2 May 2024; accepted 22 May 2024; published 26 June 2024)

Efficient and tunable qubit unidirectional routers and spin-wave diodes play an important role in classical and quantum information processing domains. Here we reveal that multilevel neutral cold atoms can mediate both dissipative and coherent couplings. Interestingly, we investigate and practically implement this paradigm in experiments, successfully synthesizing a system with dual functionality as both a photonic qubit unidirectional router and a spin-wave diode. By manipulating the helicity of the field, we can effectively balance the coherent coupling and the dissipative channel, thereby ensuring the unidirectional transfer of photonic qubits. The qubit fidelity exceeds $(97.49 \pm 0.39)\%$, and the isolation ratio reaches 16.8 ± 0.11 dB, while the insertion loss is lower than 0.36 dB. Furthermore, we show that the spin-wave diode can effectively achieve unidirectional information transfer by our appropriately setting the coherent-coupling parameters. Our work not only provides ideas for the design of extensive components in quantum network but also opens up possibilities for non-Hermitian quantum physics, complex quantum networks, and unidirectional quantum information transfer.

DOI: [10.1103/PhysRevApplied.21.L061002](https://doi.org/10.1103/PhysRevApplied.21.L061002)

a. Introduction. In contemporary communication and information technology, the concept of unidirectional routing for information carriers has attracted substantial attention. This concept is extensively used in the transmission of various signals, including acoustic waves [1–3], radio frequencies [4,5], and quantum signals [6]. Among them, gyrators serve an indispensable role as key components in facilitating efficient and orderly information exchange between different nodes [4,7], dual-port isolators effectively suppress reverse noise [4,6,8,9], while unidirectional amplifiers focus on the directional amplification of weak signals [10,11]. In linear systems, the achievement of unidirectional responses hinges on the disruption of time-reversal symmetry through the application of real or synthetic magnetic fields. However, the practicality of these traditional unidirectional devices is hampered by their biased magnetic fields. In recent years, promising physical methods have emerged to overcome the aforementioned limitations, including nonlinear optics [12–14],

optomechanics [15,16], atomic gases [17–21], quantum dots [22], and metamaterials [23].

Unidirectional routers and spin-wave diodes simplify the intricate nature of photonic networks [8,24], augment communication-channel capacities [25,26], and are valuable resources in quantum sensing [27]. Such devices promote the development of more-efficient and more-adaptable quantum information platforms [6,28]. They have stimulated numerous recent studies on nonreciprocal couplings and chiral-magnon transfer, such as studies of quantum transistors and transducers [29–31], quantum diodes [32–34], unidirectional amplifiers [35–38], and spin-wave diodes [6,28,31,39,40]. However, as the quantum nodes increase, the cumulative effect of insertion loss and quantum coherence loss leads to a significant increase in the complexity of directional transmission and detection of quantum states between nodes [6]. Therefore, aside from large isolation, ensuring the high efficiency (low insertion loss) and high fidelity of unidirectional routers and spin-wave diodes is an important and promising research topic.

In this Letter, we present a paradigm for realizing a non-Hermitian unidirectional router (NHUR) and spin-wave diode for arbitrary photonic qubits. We consider rich multilevel neutral cold atoms as depicted in Fig. 1(a). We demonstrate that the effective interactions used in this

*Corresponding author: dds@ustc.edu.cn†Corresponding author: drshi@ustc.edu.cn

‡These authors contributed equally to this work.

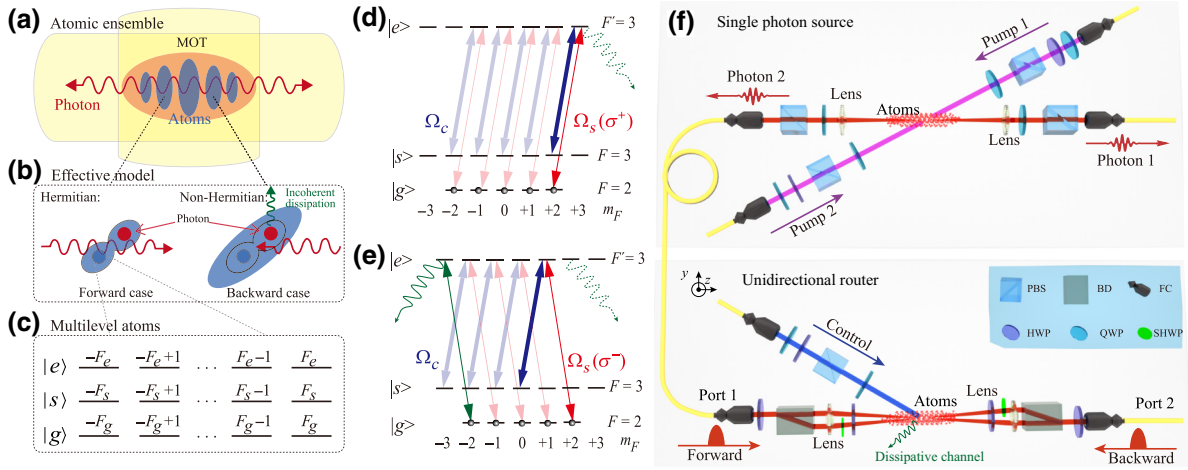


FIG. 1. Schematic and experimental setup for non-Hermitian unidirectional routing. (a) The magnon-photon interface in a cold-atom ensemble. (b) An efficient non-Hermitian interaction model between light and atoms. In forward routing, coherent coupling produces a photon-routing channel. In backward routing, incoherent coupling leads to dissipation. (c) Multilevel structure of atoms, which is composed of three states $|g\rangle$, $|s\rangle$, and $|e\rangle$ (magnons) with angular momenta F_g , F_s , and F_e , respectively. (d) In forward routing, the helicity of the control field and the helicity of the signal photon are the same, collective atomic system and photon build coherent coupling. (e) In backward routing, due to the opposite helicity of the signal photon and the control field, a magnon ($|g, m_F = -2\rangle$) generates an incoherent dissipative channel. (f) Experimental setup. The single-photon source emits a pair of heralded photons (photons 1 and 2) [41]. The unidirectional router exemplifies the non-Hermitian mechanism of unidirectional routing for photonic qubits. BD, beam displacer; FC, fiber collimator; HWP, half-wave plate; PBS, polarized beam splitter; QWP, quarter-wave plate; SHWP, small half-wave plate.

paradigm can be described by a coherent coupling balanced against the corresponding dissipative coupling. The interaction dynamics between the collective atomic states and photons are precisely manipulated through a chiral control field. [42]. The helicity and frequency detuning of the control field serve as critical controllable parameters that generate non-Hermitian behavior, thereby resulting in a unidirectional router and spin-wave diode [43]. This framework provides a perspective for investigating quantum state transfer mechanisms within chiral quantum networks and information processing domains, paving the way for further investigations [6,28,39,44–47].

b. Model and setup. Our model is based on the eigenstate structure and cooperative excitation properties arising from the collective coupling of trapped atoms, as shown in Fig. 1(b). Driven by a chiral control field, magnons and collective atomic spin waves in atoms generate a helicity-dependent incoherent dissipation channel. Balance of coherent coupling and the dissipative channel breaks the time-reversal symmetry [42,48,49]. In this scenario, dissipation profoundly alters the routing matrix, transforming it from a Hermitian to a non-Hermitian configuration [8]. This process induces directional transfer properties in the photon-atom interface.

The multilevel atoms are consisted in two metastable states $|g\rangle$ and $|e\rangle$ (magnons) and an excited state $|s\rangle$ [50,51], as shown in Fig. 1(c). The underlying directional quantum process is explained by the energy-level diagram

[Figs. 1(d) and 1(e)]. Initially, all atoms were prepared in the $|g\rangle$ state, where m_F represents the magnetic quantum number of the hyperfine states. A control field (Ω_c) drives coherence transition between $|s\rangle$ and $|e\rangle$. Signal photons couple the transition between $|g\rangle$ and $|e\rangle$. The helicity σ of the control field is fixed at 1, indicating the atomic transition from state $|s\rangle$ to state $|e\rangle$ with $\Delta m_F = 1$ [52]. The chirality of the optical field as an effective tuning knob can balance the coherent coupling and dissipative channels.

In forward routing, as depicted in Fig. 1(d), the helicity σ of the signal photon is 1. Coherent coupling exists between the signal photon and the collective atomic states, forming a stable photon channel between two states. In backward routing, the photon follows the spin-momentum locking [53–55], entailing a time-reversal operation as $\mathbf{k} \rightarrow -\mathbf{k}, \sigma \rightarrow -\sigma$, as shown in Fig. 1(e). The chiral photon induces a dissipative channel that couples the states $|g, m_F = -2\rangle$ and $|e, m_F = -3\rangle$, mediating incoherent interactions between the collective exciton and its immediate environmental surroundings [42].

In the rotating frame, we obtain the effective non-Hermitian Hamiltonian H_{eff} governing the dynamics of the magnon-photon interface in the form of [41]

$$H_{\text{eff}} = \begin{pmatrix} \Lambda & 0 & \Omega_p/2 \\ 0 & \delta & \Omega_c/2 \\ \Omega_p/2 & \Omega_c/2 & \Delta_p \end{pmatrix}, \quad (1)$$

where $\delta = \Delta_p - \Delta_c$ is the two-photon detuning, and Δ_c and Δ_p denote the detuning of the control field and the signal field, respectively. Λ determines the level of non-Hermiticity in the system (the calculated eigenvalues are complex values when Λ is nonzero [41]). In forward routing, $\Lambda = 0$, H_{eff} is a Hermitian operator. In backward routing, $\Lambda = -i\gamma_{\text{eff}}/2$, H_{eff} transforms into a non-Hermitian Hamiltonian. $\gamma_{\text{eff}} = \Omega^2/\Gamma$ arises from the incoherent dissipation, Ω is the Rabi frequency of the dissipative coupling, and Γ is the spontaneous decay rate of the state $|e\rangle$.

On the basis of the model described above, we design the experimental setup as shown in Fig. 1(f). The system consists of two components: a single-photon source and a unidirectional router. The single-photon source emits heralded Stokes (photon 1, S1) and anti-Stokes (photon 2, S2) photons [41,56–59]. S1 serves as a trigger signal, and the unidirectional router introduces S2 via port 1 or port 2 to investigate routing properties. Here we establish the z axis as the quantization axis and designate the terms “forward” and “backward” to illustrate the routing direction of S2 along the $+z$ and $-z$ axes, respectively. We use a beam displacer to displace the arbitrary qubit state ($|\psi\rangle = \cos(\theta/2)|H\rangle + e^{i\phi}\sin(\theta/2)|V\rangle$) onto a pair of orthogonal-polarization states, $|H\rangle$ and $|V\rangle$, where they are spatially separated. Then we configure the two photon paths to maintain the same helicity. After the photons have passed through the atoms, we use the reverse process to erase the path information and reconstruct the qubits. Meanwhile, the control field is incident on the atoms at 2° with respect to the signal path.

The time evolution of the density matrix ρ is described by the master equation $\dot{\rho} = -i[H_{\text{eff}}, \rho] + \mathcal{L}[\rho]$, where \mathcal{L} is the Lindblad operator describing the decay and dephasing of the atoms [41]. The signal transmission is proportional to $T = |h|^2$ [$h = \exp(-D\tilde{\chi}/2)$], where D is the optical depth of atoms. $\tilde{\chi} = \chi_{\text{EIT}} + \chi_{\text{loss}}$ is the effective chiral susceptibility of atoms, and the imaginary part of $\tilde{\chi}$ indicates the absorption [41]. χ_{EIT} illustrates the coherent coupling due to electromagnetically induced transparency (EIT) [49,60]. χ_{loss} accounts for incoherent dissipation, which could result in photon losses [41,42,61].

By solving the master equation, we derive the chiral susceptibility within the theoretical framework. In forward routing, $\chi_{\text{loss}} = 0$, the effective chiral susceptibility is determined solely by the coherent coupling, taking the form [41]

$$\tilde{\chi}_{1 \rightarrow 2} = \chi_{\text{EIT}}^{1 \rightarrow 2} = \sum_{i=-2}^2 \eta G_{i+1,i} \rho_{i+1,i}. \quad (2)$$

In backward routing, dissipative channels and coherent coupling compete with each other, and the effective susceptibility is given by

$$\tilde{\chi}_{2 \rightarrow 1} = \chi_{\text{EIT}}^{2 \rightarrow 1} + \chi_{\text{loss}}^{2 \rightarrow 1} \quad (3)$$

$$= \sum_{i=-2}^2 \eta G_{i-1,i} \rho_{i-1,i} + \eta G_{-3,-2} \rho_{-3,-2}, \quad (4)$$

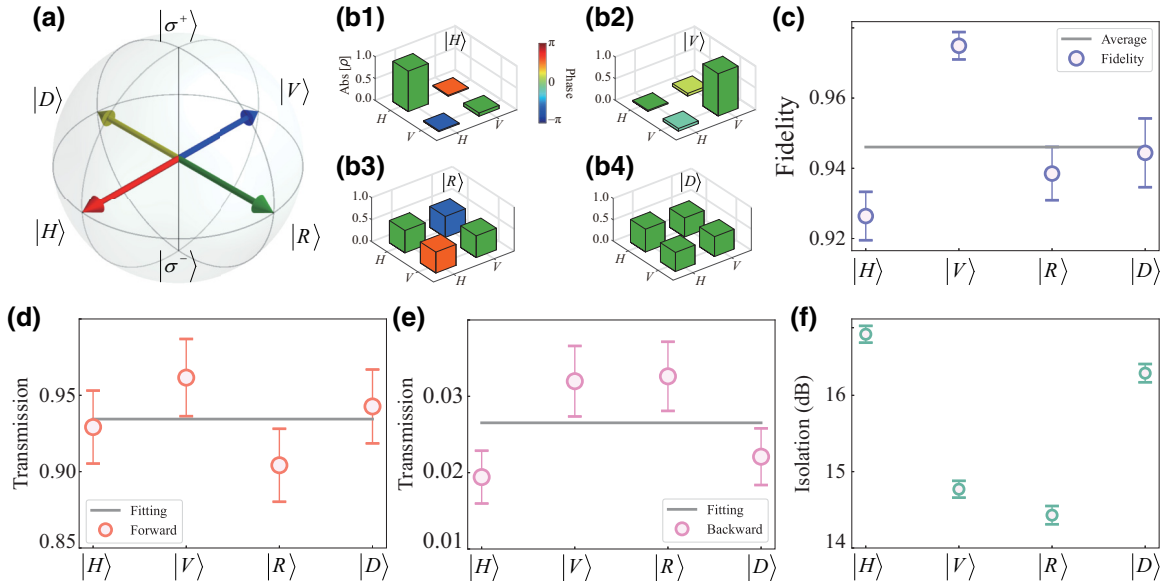


FIG. 2. Transmission properties of photonic qubits. (a) Poincaré-sphere representation of photonic qubits. (b) Reconstructed density matrices of photonic qubits (b1) $|H\rangle$, (b2) $|V\rangle$, (b3) $|R\rangle$, and (b4) $|D\rangle$ after they have passed through the NHUR along the forward routing. The height of the bars signifies the absolute value of ρ , and the color indicates the phase of the density-matrix elements. (c) Fidelity of the four photonic qubits. (d),(e) The routing properties of photonic qubits are observed in the NHUR apparatus, where (d),(e) correspond to the forward routing and the backward routing, respectively. The gray lines represent the theoretical fitting. (f) Isolation ratio of the photonic qubits. The error bars are estimated from Poisson statistics and represent ± 1 standard deviation.

where η depends on the initial atomic population and $G_{mn} = 2N|\mu_{e_m, g_n}|^2/\hbar\epsilon_0$ describes the atom-photon interaction coefficient, where μ_{e_m, g_n} is the dipole moment for the transitions $|g, m_F = m\rangle \rightarrow |e, m_F' = n\rangle$ ($m \in \{-3, 3\}$, $n \in \{-2, 2\}$) [62].

c. Unidirectional router. The Poincaré sphere of four photonic states $|i\rangle$ is depicted in Fig. 2(a), where $i = \{H, V, R, D\}$. Using quantum state tomography [41,63], as depicted in Fig. 2(b), we obtain the reconstructed density matrices for the forward-transmitted qubits. The fidelity metrics of the four qubits are denoted as $\mathcal{F}_i = \{0.92, 0.97, 0.93, 0.94\}$, as illustrated in Fig. 2(c).

The directional transmission rates T_i of the four qubits are shown in Figs. 2(d) and 2(e). In forward routing, the coherent coupling leads to a high transmission $T_i^{1 \rightarrow 2} = \{0.93, 0.96, 0.94, 0.94\}$. As expected, the backward transmission remains negligibly small, with $T_i^{2 \rightarrow 1} = \{0.019, 0.032, 0.033, 0.022\}$. In Fig. 2(f), we show the calculated isolation ratios of the four qubits [41], and have $I_i = \{16.80, 14.77, 14.43, 16.29\}$ dB. The insertion loss is defined as $-10 \ln(T^{1 \rightarrow 2})$, and we calculate the insertion loss of the four qubits as $\{0.36, 0.18, 0.27, 0.27\}$ dB. The noisy photons produced by the spontaneous-Raman-scattering process in atoms are the main factor limiting our isolation ratio, and the signal-to-noise ratio of signal photons can be further increased by use of an optical cavity [20].

d. Spin-wave diode. We further achieve a spin-wave diode at the magnon-photon interface by using chiral control pulses (write and readout pulses). Driven by the write pulse, photonic qubits ($|H\rangle$) are converted into collective-excitation spin-wave excitons through EIT and are stored in atoms in the form of magnons [64,65], as illustrated in Fig. 3(a). After a storage time of 500 ns, the magnons are reconverted into qubits through readout pulses, with both the write pulses and the readout pulses having a duration of 1 μ s. In forward routing, we obtain the retrieved qubit as illustrated in Fig. 3(b). In Fig. 3(c), no retrieved qubit can be obtained in the backward routing due to the incoherent dissipative channel. The directional-state-transfer process described above can thus be functioned as a spin-wave diode. This process filters out incoherent noise, while protecting the quantum information from unwanted backaction noise [6]. Spin-wave diodes also have great potential in various areas, including directional state transfer in chiral quantum networks [6,44], the design of quantum circuits [28,45,46], and the generation of entanglement [39,47], and provide a fertile ground for research into quantum many-body systems and collective effects [6].

e. Tunable dynamic properties. We next investigate the dynamical properties of the unidirectional router. From the theoretical model, the parameters δ/Γ and D play an important role in balancing the coherent coupling and the dissipative channel. We theoretically

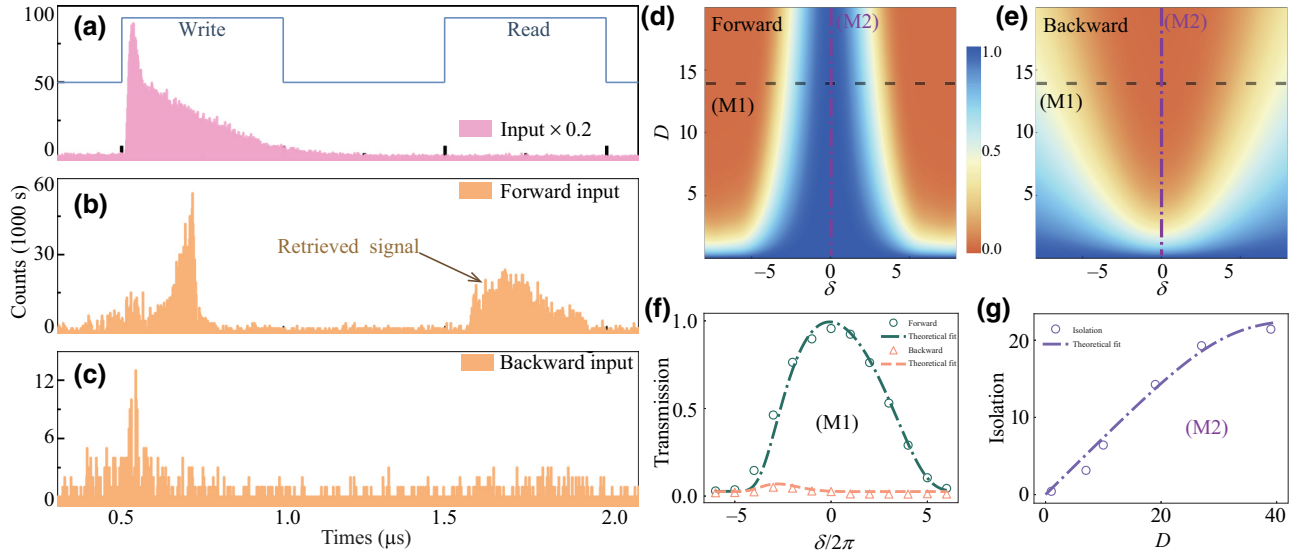


FIG. 3. Spin-wave diode and dynamical properties of the NHUR apparatus. (a) Input wave packet of a photonic qubit before the NHUR. The blue line represents the temporal sequence of the control field. (b),(c) Retrieved signals of the NHUR in forward routing and backward routing (c), respectively. (d),(e) Output-signal spectrum for forward routing and backward routing, respectively, as a function of optical depth D and frequency detuning δ . The dynamical properties of the NHUR experiment, observed at specific parameter-configuration locations M1 and M2, are represented by dashed and dotted lines in (f),(g), respectively. (f) Transmission spectrum for forward routing (green circles) and backward routing (orange triangles) obtained by our scanning the control-field detuning δ . The dotted green line and dashed orange line represent the fitting results obtained at M1 ($D = 14$). (g) Isolation ratio of the NHUR versus D , with the control-field detuning $\delta = 0$. The dotted line represents a fitting derived from theoretical expectations.

calculated the expected unidirectional qubit transfer for δ and D .

Figures 3(d) and 3(e) depict theoretical-calculation results for the forward-routing transmission and the backward-routing transmission, respectively. We examine the experimental observations [in Fig. 3(f)] at feature position M1, as indicated by the dotted line in Fig. 3(d). With a far-detuned control field, i.e., $\tilde{\chi}_{1\rightarrow 2} \approx \tilde{\chi}_{2\rightarrow 1} \approx -1/\delta$, the atoms absorb bidirectional signal photons. When $\delta = 0$, the system breaks time-reversal symmetry, leading to the emergence of extreme values of the direction-dependent transfer coefficients, i.e., $h_{1\rightarrow 2} \approx 1$ and $h_{2\rightarrow 1} \approx 0$. In the vicinity of $\Delta\omega_p \sim 0$ MHz, we observe significantly high transmission and nearly negligible transmission in the forward routing and the backward routing, respectively. This results in a high forward (low backward) transmission rate of $(92.9 \pm 2.0)\%$ [$(2.6 \pm 0.4)\%$]. Figure 3(g) represents the observation result for the dotted line M2. Limited by our experimental setup, the isolation ratio of the NHUR can reach 20 dB when $D = 40$. Theoretically, the isolation can be improved by use of a higher D . Thus, the NHUR process with increased D can be treated as a sequence of spatially cascaded collective-exciton-mode-based NHURs.

In Fig. 4, we investigate the tunable properties of the NHUR process with a fixed signal helicity. We initialized the photonic qubits in two states: $|H\rangle$ (represented by purple stars) for the forward direction and $|V\rangle$ (represented by yellow triangles) for the backward direction. By continuously adjusting the helicity of the control field [41], we can dynamically manipulate the qubit transfer direction. The inclusion of the above-mentioned feature underpins applications of the unidirectional router within the realm of

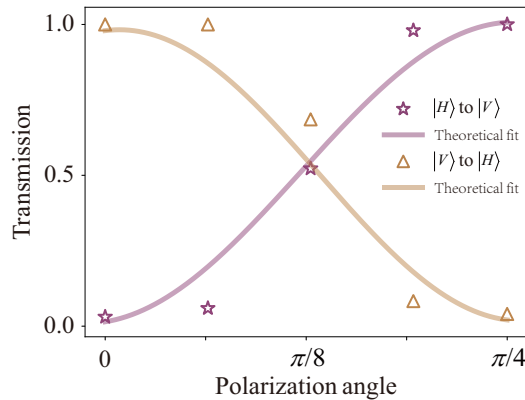


FIG. 4. Tunable properties of the dissipation-induced NHUR. The input photonic qubits are initially prepared in $|H\rangle$ (purple star) and $|V\rangle$ (yellow triangle) states. The unidirectional transmission characteristics of the NHUR can be reversed by manipulation of the chirality of the control field. Purple stars and yellow triangles correspond to the control field with helicity $\sigma = +1$ and $\sigma = -1$, respectively. The solid curves represent theoretical-fit results.

quantum information processing by providing a new angle for realizing universal quantum gates [66,67].

f. Conclusion. In summary, we investigated the Hamiltonian describing photon-atom interaction, demonstrating that multilevel atoms can mediate coherent and dissipative couplings. When coherent coupling and dissipative channels are balanced, we obtain a polarization-independent unidirectional router and spin-wave diode. Experimental results show that our approach enables high-fidelity, high-isolation, and low-insertion-loss directional transmission of arbitrarily polarized qubits. Additionally, the spin-wave diode facilitates directional quantum state transfer. This mechanism can be triggered by light fields, magnetic fields, and acoustic waves, potentially coupling with various energy modes. Our theoretical framework is expected to apply to physical systems characterized by rich energy-level structures, including various similar systems such as molecules, nitrogen-vacancy centers, trapped ions, and optical microresonators [68–75]. Our work not only provides a new perspective for creating effective noncoherent dissipative channels and promotes effective control of the system Hamiltonian but also paves the way for designing quantum diodes and improving existing unidirectional routers [6].

Acknowledgments. We thank Professor Franco Nori, Professor Ke-Yu Xia, Professor Wei Yi, Professor Wei Zhang, Dr. Ying-Hao Ye, Dr. Wei-Hang Zhang, and Dr. Lei Zeng for fruitful discussions. This work was supported by the National Key Research and Development Program of China (Grant No. 2022YFA1404002), the National Natural Science Foundation of China (Grants No. U20A20218 and No. 11934013), the Major Science and Technology Projects in Anhui Province (Grant No. 202203a13010001), the Youth Innovation Promotion Association of the Chinese Academy of Sciences (Grant No. 2018490), the Innovation Program for Quantum Science and Technology (Grant No. 2021ZD0301100), and Anhui Initiative in Quantum Information Technologies (Grant No. AHY020200).

- [1] T. Devaux *et al.*, Acoustic radiation pressure for nonreciprocal transmission and switch effects, *Nat. Commun.* **10**, 3292 (2019).
- [2] Q. Wang *et al.*, Acoustic topological beam nonreciprocity via the rotational Doppler effect, *Sci. Adv.* **8**, eabq4451 (2022).
- [3] L. Hackett *et al.*, Non-reciprocal acoustoelectric microwave amplifiers with net gain and low noise in continuous operation, *Nat. Electron.* **6**, 76 (2023).
- [4] A. Nagulu *et al.*, Non-reciprocal electronics based on temporal modulation, *Nat. Electron.* **3**, 241 (2020).
- [5] L. Shao *et al.*, Electrical control of surface acoustic waves, *Nat. Electron.* **5**, 348 (2022).
- [6] P. Lodahl *et al.*, Chiral quantum optics, *Nature* **541**, 473 (2017).
- [7] G. Viola and D. P. DiVincenzo, Hall effect gyrators and circulators, *Phys. Rev. X* **4**, 021019 (2014).
- [8] D. Jalas *et al.*, What is and what is not an optical isolator, *Nat. Photonics* **7**, 579 (2013).

- [9] M. Scheucher *et al.*, Quantum optical circulator controlled by a single chirally coupled atom, *Science* **354**, 1577 (2016).
- [10] C. C. Wanjura *et al.*, Topological framework for directional amplification in driven-dissipative cavity arrays, *Nat. Commun.* **11**, 3149 (2020).
- [11] Z. Shen *et al.*, Reconfigurable optomechanical circulator and directional amplifier, *Nat. Commun.* **9**, 1797 (2018).
- [12] L. Fan *et al.*, An all-silicon passive optical diode, *Science* **335**, 447 (2012).
- [13] Q.-T. Cao *et al.*, Experimental demonstration of spontaneous chirality in a nonlinear microresonator, *Phys. Rev. Lett.* **118**, 033901 (2017).
- [14] K. Xia *et al.*, Cavity-free optical isolators and circulators using a chiral cross-Kerr nonlinearity, *Phys. Rev. Lett.* **121**, 203602 (2018).
- [15] S. Manipatruni *et al.*, Optical nonreciprocity in optomechanical structures, *Phys. Rev. Lett.* **102**, 213903 (2009).
- [16] Z. Shen *et al.*, Experimental realization of optomechanically induced non-reciprocity, *Nat. Photonics* **10**, 657 (2016).
- [17] E.-Z. Li *et al.*, Experimental demonstration of cavity-free optical isolators and optical circulators, *Phys. Rev. Res.* **2**, 033517 (2020).
- [18] M.-X. Dong *et al.*, All-optical reversible single-photon isolation at room temperature, *Sci. Adv.* **7**, eabe8924 (2021).
- [19] S. Zhang *et al.*, Thermal-motion-induced non-reciprocal quantum optical system, *Nat. Photonics* **12**, 744 (2018).
- [20] X.-X. Hu *et al.*, Noiseless photonic non-reciprocity via optically-induced magnetization, *Nat. Commun.* **12**, 2389 (2021).
- [21] S. Pucher *et al.*, Atomic spin-controlled non-reciprocal Raman amplification of fibre-guided light, *Nat. Photonics* **16**, 380 (2022).
- [22] N. O. Antoniadis *et al.*, A chiral one-dimensional atom using a quantum dot in an open microcavity, *npj Quantum Inf.* **8**, 27 (2022).
- [23] P. P. Iyer *et al.*, Unidirectional luminescence from InGaN/GaN quantum-well metasurfaces, *Nat. Photonics* **14**, 543 (2020).
- [24] A. Metelmann and H. Türeci, Nonreciprocal signal routing in an active quantum network, *Phys. Rev. A* **97**, 043833 (2018).
- [25] D. A. Miller, Are optical transistors the logical next step?, *Nat. Photonics* **4**, 3 (2010).
- [26] E. Verhagen and A. Alù, Optomechanical nonreciprocity, *Nat. Phys.* **13**, 922 (2017).
- [27] H.-K. Lau and A. A. Clerk, Fundamental limits and non-reciprocal approaches in non-Hermitian quantum sensing, *Nat. Commun.* **9**, 4320 (2018).
- [28] H. J. Kimble, The quantum internet, *Nature* **453**, 1023 (2008).
- [29] H. Gorniaczyk *et al.*, Single-photon transistor mediated by interstate Rydberg interactions, *Phys. Rev. Lett.* **113**, 053601 (2014).
- [30] Z. Wang *et al.*, An ultra-high gain single-photon transistor in the microwave regime, *Nat. Commun.* **13**, 6104 (2022).
- [31] K. Stannigel *et al.*, Optomechanical transducers for long-distance quantum communication, *Phys. Rev. Lett.* **105**, 220501 (2010).
- [32] A. R. Hamann *et al.*, Nonreciprocity realized with quantum nonlinearity, *Phys. Rev. Lett.* **121**, 123601 (2018).
- [33] C. Müller *et al.*, Nonreciprocal atomic scattering: A saturable, quantum Yagi-Uda antenna, *Phys. Rev. A* **96**, 053817 (2017).
- [34] S. Barzanjeh *et al.*, Manipulating the flow of thermal noise in quantum devices, *Phys. Rev. Lett.* **120**, 060601 (2018).
- [35] A. Metelmann and A. A. Clerk, Nonreciprocal photon transmission and amplification via reservoir engineering, *Phys. Rev. X* **5**, 021025 (2015).
- [36] F. Lecocq *et al.*, Nonreciprocal microwave signal processing with a field-programmable Josephson amplifier, *Phys. Rev. Appl.* **7**, 024028 (2017).
- [37] G. A. Peterson *et al.*, Demonstration of efficient nonreciprocity in a microwave optomechanical circuit, *Phys. Rev. X* **7**, 031001 (2017).
- [38] D. Malz *et al.*, Quantum-limited directional amplifiers with optomechanics, *Phys. Rev. Lett.* **120**, 023601 (2018).
- [39] J. I. Cirac *et al.*, Quantum state transfer and entanglement distribution among distant nodes in a quantum network, *Phys. Rev. Lett.* **78**, 3221 (1997).
- [40] J. Lan *et al.*, Spin-wave diode, *Phys. Rev. X* **5**, 041049 (2015).
- [41] See Supplemental Material at <http://link.aps.org/supplemental/10.1103/PhysRevApplied.21.L061002> for more details.
- [42] R. Wen *et al.*, Non-Hermitian magnon-photon interference in an atomic ensemble, *Phys. Rev. Lett.* **122**, 253602 (2019).
- [43] J. Simon *et al.*, Single-photon bus connecting spin-wave quantum memories, *Nat. Phys.* **3**, 765 (2007).
- [44] G.-S. Ye *et al.*, A photonic entanglement filter with Rydberg atoms, *Nat. Photonics* **17**, 538 (2023).
- [45] D.-S. Ding *et al.*, Raman quantum memory of photonic polarized entanglement, *Nat. Photonics* **9**, 332 (2015).
- [46] Y.-W. Cho and Y.-H. Kim, Atomic vapor quantum memory for a photonic polarization qubit, *Opt. Express* **18**, 25786 (2010).
- [47] C. Gonzalez-Ballesteros *et al.*, Chiral route to spontaneous entanglement generation, *Phys. Rev. B* **92**, 155304 (2015).
- [48] A. V. Gorshkov *et al.*, Universal approach to optimal photon storage in atomic media, *Phys. Rev. Lett.* **98**, 123601 (2007).
- [49] L.-M. Duan *et al.*, Long-distance quantum communication with atomic ensembles and linear optics, *Nature* **414**, 413 (2001).
- [50] Y.-C. Chen *et al.*, Roles of degenerate Zeeman levels in electromagnetically induced transparency, *Phys. Rev. A* **61**, 053805 (2000).
- [51] B. Wang *et al.*, Controlling the polarization rotation of an optical field via asymmetry in electromagnetically induced transparency, *Phys. Rev. A* **73**, 051801 (2006).
- [52] F. Alpegiani *et al.*, Electromagnetic helicity in complex media, *Phys. Rev. Lett.* **120**, 243605 (2018).
- [53] K. Y. Bliokh *et al.*, Magnetoelectric effects in local light-matter interactions, *Phys. Rev. Lett.* **113**, 033601 (2014).
- [54] T. Van Mechelen and Z. Jacob, Universal spin-momentum locking of evanescent waves, *Optica* **3**, 118 (2016).
- [55] Z.-Q. Yang *et al.*, Spin-momentum-locked edge mode for topological vortex lasing, *Phys. Rev. Lett.* **125**, 013903 (2020).
- [56] V. Balić *et al.*, Generation of paired photons with controllable waveforms, *Phys. Rev. Lett.* **94**, 183601 (2005).
- [57] S. Du *et al.*, Narrowband biphoton generation near atomic resonance, *JOSA B* **25**, C98 (2008).
- [58] D.-S. Ding *et al.*, Single-photon-level quantum image memory based on cold atomic ensembles, *Nat. Commun.* **4**, 2527 (2013).
- [59] P. Grangier *et al.*, Experimental evidence for a photon anticorrelation effect on a beam splitter: A new light on single-photon interferences, *EPL (Europhys. Lett.)* **1**, 173 (1986).
- [60] V. Tiwari *et al.*, Electromagnetically induced transparency in cold ⁸⁵Rb atoms trapped in the ground hyperfine $F = 2$ state, *J. Phys. B: At., Mol. Opt. Phys.* **43**, 095503 (2010).
- [61] M. Fleischhauer *et al.*, Electromagnetically induced transparency: Optics in coherent media, *Rev. Mod. Phys.* **77**, 633 (2005).
- [62] D. A. Steck, Rubidium 87 D line data (2001).
- [63] D. F. V. James *et al.*, Measurement of qubits, *Phys. Rev. A* **64**, 052312 (2001).
- [64] M. Fleischhauer and M. D. Lukin, Dark-state polaritons in electromagnetically induced transparency, *Phys. Rev. Lett.* **84**, 5094 (2000).
- [65] C.-H. Dong *et al.*, Brillouin-scattering-induced transparency and non-reciprocal light storage, *Nat. Commun.* **6**, 6193 (2015).
- [66] K. Koshino *et al.*, Deterministic photon-photon SWAP gate using a Λ system, *Phys. Rev. A* **82**, 010301 (2010).
- [67] L.-M. Duan and H. Kimble, Scalable photonic quantum computation through cavity-assisted interactions, *Phys. Rev. Lett.* **92**, 127902 (2004).
- [68] B. Pingault *et al.*, All-optical formation of coherent dark states of silicon-vacancy spins in diamond, *Phys. Rev. Lett.* **113**, 263601 (2014).
- [69] L. J. Rogers *et al.*, All-optical initialization, readout, and coherent preparation of single silicon-vacancy spins in diamond, *Phys. Rev. Lett.* **113**, 263602 (2014).
- [70] K. Xia *et al.*, Quantum routing of single optical photons with a superconducting flux qubit, *Phys. Rev. A* **97**, 052315 (2018).
- [71] M.-M. Cao *et al.*, Probing complex-energy topology via non-Hermitian absorption spectroscopy in a trapped ion simulator, *Phys. Rev. Lett.* **130**, 163001 (2023).
- [72] H. Cao and J. Wiersig, Dielectric microcavities: Model systems for wave chaos and non-Hermitian physics, *Rev. Mod. Phys.* **87**, 61 (2015).
- [73] R. El-Ganainy *et al.*, Non-Hermitian physics and PT symmetry, *Nat. Phys.* **14**, 11 (2018).
- [74] S. Bernon *et al.*, Manipulation and coherence of ultra-cold atoms on a superconducting atom chip, *Nat. Commun.* **4**, 2380 (2013).
- [75] L. Zhu *et al.*, A dielectric metasurface optical chip for the generation of cold atoms, *Sci. Adv.* **6**, eabb6667 (2020).